Multiparametric investigation of North Sea particulate matter. Preliminary results in the Skagerrak

Particulate matter
North Sea
Granulometry
Scanning electron microscopy
Neutron activation analysis

Matière particulaire
Mer du Nord
Granulométrie
Microscopie électronique à balayage
Analyse par activation neutronique

Dominique BOUST [a], **Jean-Paul DUPONT** [b], **Philippe BIENVENU** [a], **Ulah EZAT** [c], **Robert LAFITE** [b], **Thierry LEBOULANGER** [b], **Charlotte VINCHON** [d], **Francis ALBAREDE** [e]

[a] Laboratoire de Radioécologie Marine, CEA IPSN DPEI SERE, Centre de la Hague, B.P. 508, 50105 Cherbourg Cedex, France.

[b] Laboratoire de Géologie, Université de Rouen, 76230 Mont-Saint-Aignan, France.

[c] Centre des Faibles Radioactivités, CNRS, B.P. 1, 91190 Gif-sur-Yvette, France.

[d] SGN/GRF, Bureau de Recherches Géologiques et Minières, B.P. 6009, 45060 Orléans, France.

[e] CRPG, Centre National de la Recherche Scientifique, B.P. 20, 54501 Vandœuvre-les-Nancy Cedex, France.

ABSTRACT

During the *Tramanor* cruise, in July 1988, seawater and particle samples were collected along a vertical profile (530 m depth) located in the Skagerrak, a crossing-area for different water-masses and particle pools. A sampling strategy was developed to ensure the homogeneity of the different sets of subsamples subjected to analysis by closely-coupled complementary techniques: turbidimetry, granulometry, scanning electron microscope (SEM) observations, Tracor analyses, particulate organic carbon and nitrogen measurements, neutron activation analysis (NAA). The Baltic outflow is found in the topmost 20 m water-column (salinity ≈ 23.5; temperature ≈ 18°C) overlying North Sea waters (salinity ≈ 35; temperature ≈ 6°C). Surface waters undergo a plankton bloom, dominated by Dinoflagellates and Coccolithophoridae. The former, characterized by high C/N ratios (≈ 15; cellulosic thecae), play a significant role in the biological recycling of Zn. The latter accumulate over the halocline as typically observed in frontal structures. The detrital phase mainly consists of clay minerals which do not display important mineralogical change throughout the water-column as evidenced by the good correlation between Sc (or Al) and clay abundance determined by counting on SEM photographs. Manganese is highly enriched relative to shale-type material together with Fe, Co and Zn. The carrier phases of this Mn excess are identified by SEM + electron microprobe observations as being authigenic particles of different types: ring structures, flowerlike and rodlike particles. Here again, a close correlation is observed between Mn excess (measured by NAA) and Mn-rich particle abundances (determined by counting). These particles are partly advected; another part is generated locally by active Mn bottom recycling and subsequent co-precipitation on to particles.

Oceanologica Acta, **1991**. Proceedings of the International Colloquium on the environment of epicontinental seas, Lille, 20-22 March, 1990, **vol. sp. n°11**, 233-246.

RÉSUMÉ

Étude multiparamétrique des particules en Mer du Nord : résultats préliminaires dans le Skagerrak

Au cours de la campagne *Tramanor*, en juillet 1988, des échantillons d'eau de mer et de particules ont été prélevés sur un profil vertical (530 m de profondeur) situé dans le Skagerrak, point de rencontre de masses d'eau et de particules d'origine différente. Une stratégie d'échantillonnage a été développée pour assurer l'homogénéité des sous-échantillons destinés à l'analyse par des techniques complémentaires et étroitement couplées : turbidimétrie, granulométrie, observations au microscope électronique à balayage (MEB), analyse par Tracor, mesures de carbone et azote organiques particulaires, analyse par activation neutronique (AAN). La veine d'eau baltique occupant les vingt mètres supérieurs du profil (salinité ≈ 23,5 ; température ≈ 18°C) se superpose à des eaux de la Mer du Nord (salinité ≈ 35; température ≈ 6°C). Le bloom planctonique rencontré dans les eaux de surface est dominé par les dinoflagellés et les coccolithophoridae. Les premiers jouent un rôle important dans le recyclage du Zn. Les seconds s'accumulent au-dessus de l'halocline comme on l'observe souvent dans les structures frontales. La phase détritique est principalement constituée d'argiles dont la composition minéralogique ne semble pas évoluer en profondeur, comme le démontre la bonne corrélation existant entre Sc (ou Al) et l'abondance des argiles mesurée par comptage sur les clichés obtenus au MEB. Le manganèse est très enrichi par rapport aux shales, ainsi que Fe, Co et Zn. Les phases porteuses de cet excès de Mn sont identifiées ; il s'agit de particules authigènes de différents types : anneaux, bâtonnets, rosettes. Là encore, on observe une étroite corrélation entre l'excès de Mn et l'abondance des particules enrichies en Mn. Celles-ci sont soit advectées, soit générées sur place par diffusion de Mn dissous depuis les eaux interstitielles et précipitation sur les particules.

Oceanologica Acta, **1991**. Actes du Colloque international sur l'environnement des mers épicontinentales, Lille, 20-22 mars 1990, **vol. sp. n°11**, 233-246.

INTRODUCTION

An overview of the literature reveals the scarcity of data concerning the suspended particulate matter in the North Sea (Eisma and Kalf, 1987) and the lack of data on trace elements except some heavy metals (*see* Salomons *et al.*, 1988). Furthermore, no integrated study closely linking physical and chemical analyses and SEM imagery is available at present. The work of Eisma (1981) is an almost unique attempt in this direction. The general circulation of North Sea water masses has been investigated by different approaches using drifting buoys, modelling and, more recently, artificial radionuclides but no data exist on particle source-terms. Another problem is that poorly known local processes prevent a clear understanding of the general circulation of particles and of associated trace elements and radionuclides.

We present here preliminary results which are part of a general study of the North Sea particulate matter carried out during the *Tramanor* cruise in July 1988, supported by the *Commissariat à l'Énergie Atomique* and the *Centre National de la Recherche Scientifique* (*GDR Manche*). These data have been obtained in the Skagerrak which is a key-point, being a crossing-area for particles of various origins: southern North Sea, Baltic Sea and North Atlantic Ocean.The sampling strategy was developed in order to obtain physical and geochemical parameters as well as SEM imagery on the same samples of suspended matter.

ENVIRONMENTAL SETTING

The Skagerrak is a deep marine basin between the North and Baltic seas, primarily opened towards the former. The water depth can reach more than 700 m in its central part (Fig. 1); it is from far the deepest water over the North Sea. This is an area of particularly low tidal flow but wind stress and density differences can induce stronger currents (20 cm s^{-1} on average and up to 90 cm s^{-1}; Dahl, 1978), especially in the upper 100 m water column. Atlantic water enters the North Sea between Norway and Shetlands and becomes a subsurface current east of the Shetlands, flowing down along the western slope of the Norwegian Channel to the Skagerrak (Dooley, 1974), inducing a subsurface flow in the opposite direction of the surface flow. Due to the general low energy conditions encountered throughout the water column and the water depth, the Skagerrak is one of the main sink of suspended matter together with Kattegat and Norwegian Channel (Eisma and Kalf, 1987).

At the boundary with the Kattegat, there is an inflow of fresh water from the Baltic Sea on top. The deep flow of Skaggerak water to the Kattegat is mixed with this fresh water; this induces a surface flow of brackish water from the Kattegat. This Baltic outflow can be recognized off Swedish then Norwegian coast as a narrow coastal current. The general circulation scheme has been shown to be wind-influenced (Moller and Svansson, 1978).

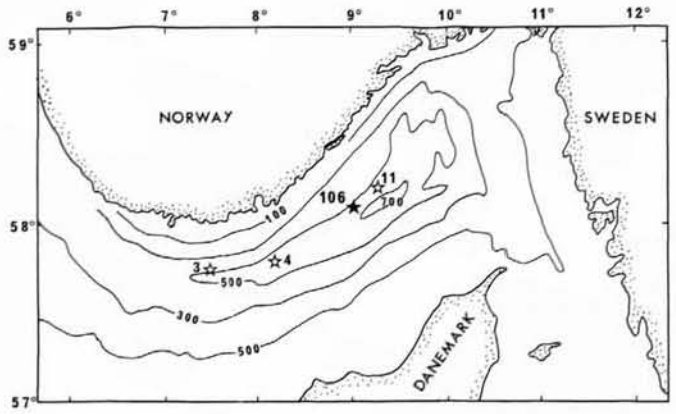

Figure 1

Location of station 106 and bathymetry of the Skagerrak. Stations 3, 4 and 11 refer to the work of Rajendran (1986).

Localisation de la station 106 et bathymétrie dans le Skagerrak. Les stations 3, 4 et 11 se rapportent au travail de Rajendran (1986).

The extent to which North Atlantic water reaches the Skagerrak has been discussed by Furnes *et al.* (1986) but is not yet clearly known. In addition, Ljøen and Svansson (1972) have shown that cooled waters flowing off the Danish coast from the North Sea shelf can cascade into the Skagerrak. This cold and heavy North Sea water, which first appears as a subsurface bulk at the edge of the Jutland Bank, continuously sinks to the deepest waters of the Skagerrak. This situation typically occurs from March to August (Ljøen, 1981). From these hydrological considerations, it clearly appears that various and time-changing particle sources and biogeochemical processes are likely to be encountered in the area.

MATERIAL AND METHODS

On-board and land-based handling and analyses are summarized in the flow-diagram shown in Figure 2.

On-board sampling and analyses

- Seawater samples were collected with 10 l Niskin bottles, mounted on a Rosette device together with a Guildline CTD probe, in order to obtain continuous salinity-temperature profiles; in addition, salinity measurements were calibrated by on-board analyses using potentiometric titration. Seawater collection was performed during the upcast of the sampler at depths selected from temperature-salinity characteristics.

- Subsamples were collected from the Niskin bottles immediately upon their arrival on deck in order to characterize the suspended matter; the following parameters were measured: turbidity (results expressed in NTU) and grain-size distribution using a Coulter counter. Grain-size analyses were performed with an 280 µm aperture; the electrolytic medium was the sea water itself after on-board calibration from Coulter standards and filtered sea water from each site. From these measurements, three parameters were obtained: 1) the particle concentrations in 16 size-fractions between 3 and 123 µm (spherical-equivalent diameter), expressed as number of particles per litre; 2) the total volume of particles per litre, expressed in $mm^3\ l^{-1}$; 3) the percentage of the total volume of the particles in each of the 16 size-fractions.

- Particle samples devoted to SEM observations were recovered on Millipore filters (0.45 µm pore diameter), rinsed with Milli-Q water, then stored at -18°C. Dry particle samples for neutron activation analyses were collected on pre-washed and pre-weighed Nuclepore filters (0.45 µm pore diameter) then rinsed with Milli-Q water and allowed to dry at room temperature under a laminar flow bench. Another set of samples was obtained on calcined glass-fibre filters for further particulate organic carbon and nitrogen analyses, and stored at -18°C. All the subsampling and storage operations were carried out in a clean lab container equipped for this cruise.

Land-based analyses

Back again on land, Millipore filters were dried at 60°C and gold-plated for SEM observations. Thus, the validity of the Coulter counter data was checked and the nature of the particles in each size-fraction was determined. Nuclepore filters were allowed to dry in a low pressure desiccator and afterwards weighed for suspended load determination. The filters were split into two parts (0.5-2 mg of particles on each). One half-filter was prepared for

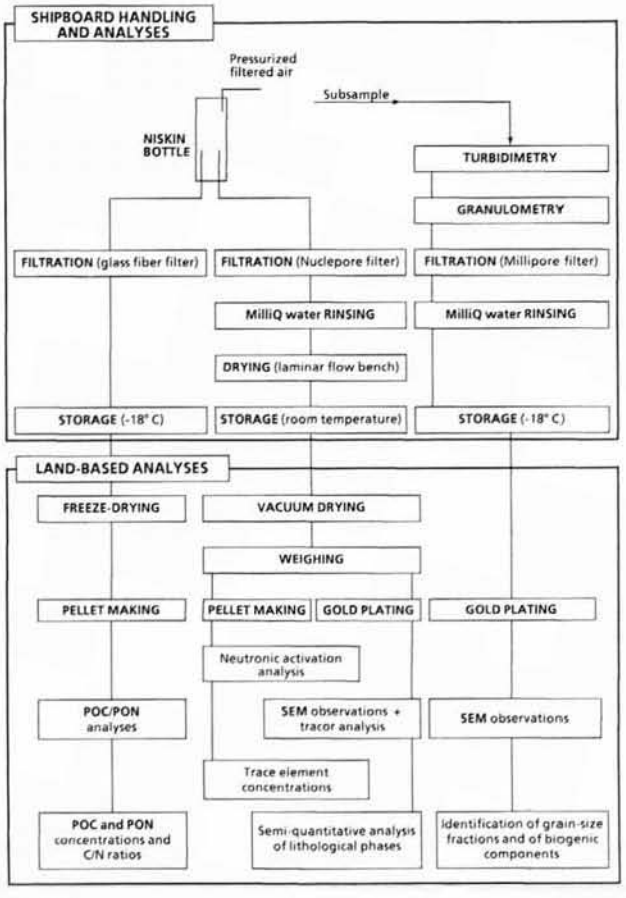

Figure 2

Flow diagram of particulate sampling and analyses.

Organigramme pour l'échantillonnage et les analyses de particules.

NAA in the Orphée reactor at Saclay. The neutron flux available is 10^{13} n cm^{-2} s^{-1}. Two activations of each sample were performed at one month minimum interval: the first, lasting 30 seconds, enabled us to measure Mn and Al concentrations by using a Na flux monitor; for the second one (15 minutes long), both international standard (W1) and a Co flux monitor were used; gamma-countings of generated radionuclides after one week, one and three months permitted determination of the concentrations of Sc, Cr, Fe, Co, Zn, Rb, Cs, Ba, La, Ce, Eu and Th. The analytical precision is better than 5 % for Sc, Cr, Fe, Zn, Ce, Eu and Th determinations; it is only about 20 % in the case of Rb, Cs, Ba and La. The other part of the filter is used for SEM and electron probe (Tracor) analyses; this considerably enhances the reliability of the comparison between bulk and ponctual analyses.

Glass-fibre filters were mineralized at 450°C during five minutes (carbonates are not affected in these conditions) under an oxygenated helium flow. The combustion of the gases is further performed on a CuO catalyst at 850°C. Nitrogen oxides are reduced to N_2 by a Cu catalyst at 450°C. CO_2 and N_2 are analysed by catharometry after chromatographic separation. The precision is ± 1% on 100 µg organic matter samples.

RESULTS

The Baltic outflow in July 1988

The upper-layer Skagerrak outflow has an intermittent character alternating between blocking and outbreak depending upon wind direction (Aure and Saetre, 1981). This was clearly observed in July 1988: just before we arrived at the station 106, on 13 July, the winds were blowing from the southwest, thus counteracting the Baltic Sea outflow and limiting the realm of the brackish waters in the close vicinity of the South Norwegian coasts. Ten days later, the conditions were completely different: the Baltic Sea outflow could be identified as far as the centre of the North Sea (maximal extension of the 33 g isohaline at 57° N- 2° E).

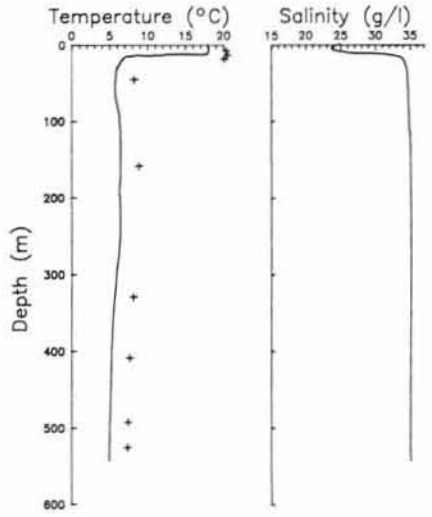

Figure 3

Temperature and salinity profiles at station 106 in July 1988 (continuous CTD profiles); symbols indicate sampling depths.

Profils de température et de salinité à la station 106 en juillet 1988 (profils CTD, en continu); les symboles indiquent les niveaux échantillonnés.

The salinity and temperature profiles (Fig. 3) reveal a well stratified water column with sharp boundaries at about 20 m depth. The temperature of the outflow waters reaches 18°C, that is 1 to 2° higher than the average temperature in this region. This results from the particularly warm and sunny weather in June 1988.

Physical characterization of suspended load and identification of particulate components

The integrated utilization of different complementary techniques (turbidimetry, granulometry, SEM, Tracor) allowed us to carry out a fine characterization of the particulate load and the identification of the lithological phases (biogenic, authigenic, detrital components) present in the different granulometric modes (Fig. 4 and 5).

We shall present here the data for each level in order to determine the main features of the particulate phases and their vertical evolution.

1 and 7 m depth

There is no important difference between these two levels except that the latter is characterized by a peak of both turbidity and suspended load. The amount of particles remains lower than 1 000 x 10^4 l^{-1} but their volume reaches 2.18 mm^3 l^{-1}, that is the maximum value of the profile. This observation indicates that the peak of turbidity at 7 m depth is primarily associated with the coarse fraction of the suspended load. The SEM observation point out that this coarse fraction (31-49 µm, Fig. 5) is essentially composed (90 %) of dinoflagellates cells (Pl.1. *a-b*)

12 m depth

The amount of particles is maximum at 1 950 x 10^4 l^{-1}. In contrast, the turbidity as well as the volume of measured particles decrease (Fig. 4). The fine fraction, between 3 and 8 µm, develops substantially. It is essentially composed of coccoliths and scarce coccospheres (*Emiliana huxleyi*; Pl. 1 *c*). This accumulation is observed just above the halocline, as described in other frontal structures (Sournia *et al.*, 1990). The abundance of the dinoflagellates in the coarse fraction is similar to that at 7 m depth (Fig. 5).

39 m depth

This level, which lies just below the frontal structure, is characterized by a significant decrease of the amount of particles (475 x 10^4 l^{-1}), of the particulate volumic concentration (0.69 mm^3 l^{-1}), and to a lesser extent of the turbidity (0.36 NTU; Fig. 4). The granulometric spectrum on figure 5 is rather flat. Three populations can be identified: 1) > 24 µm fraction, dominated by dinoflagellates, in much lower

Figure 4

Physical characterization of the suspended particulate matter at station 106.

Caractérisation physique de la matière particulaire à la station 106.

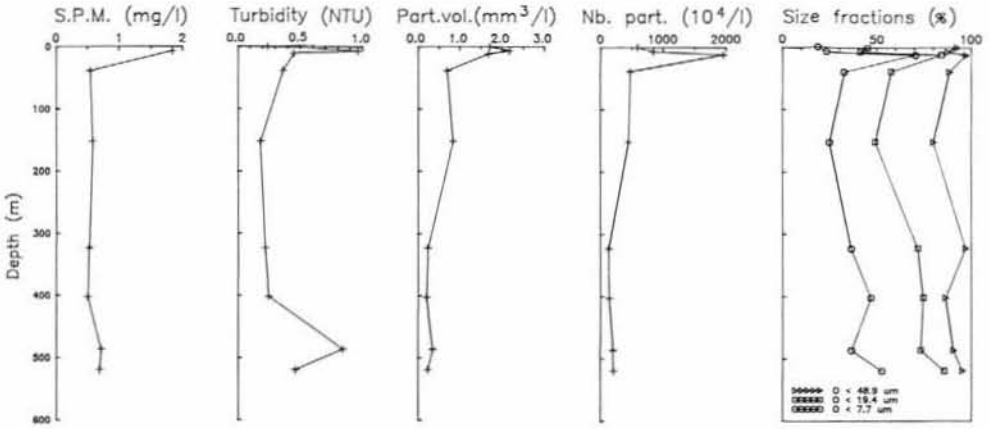

proportions than those observed above, and some diatoms, sometimes as *Chaeteroceros* rings (Pl.1. d); 2) 8-24 µm fraction: composed of diatoms, dinoflagellates (*Dinophysis* sp.), and, overall, of organic detritus (unidentified organic membranes, cellulose fibres); 3) < 8 µm fraction: composed of partially degraded coccoliths, and of clay minerals.

152 m depth

The physical parameters are of the same order of magnitude as those at 39 m depth. The populations are also similar. There is merely a slight development of the dinoflagellate population and the appearence of clay aggregates, sometimes with Fe-rich coatings (Pl. 2. *a*).

323 and 402 m depth

The particulate volume decreases (0.23 $mm^3\ l^{-1}$) because the contribution of the coarse fraction, still dominated by Dinoflagellates, becomes very small. The granulometric

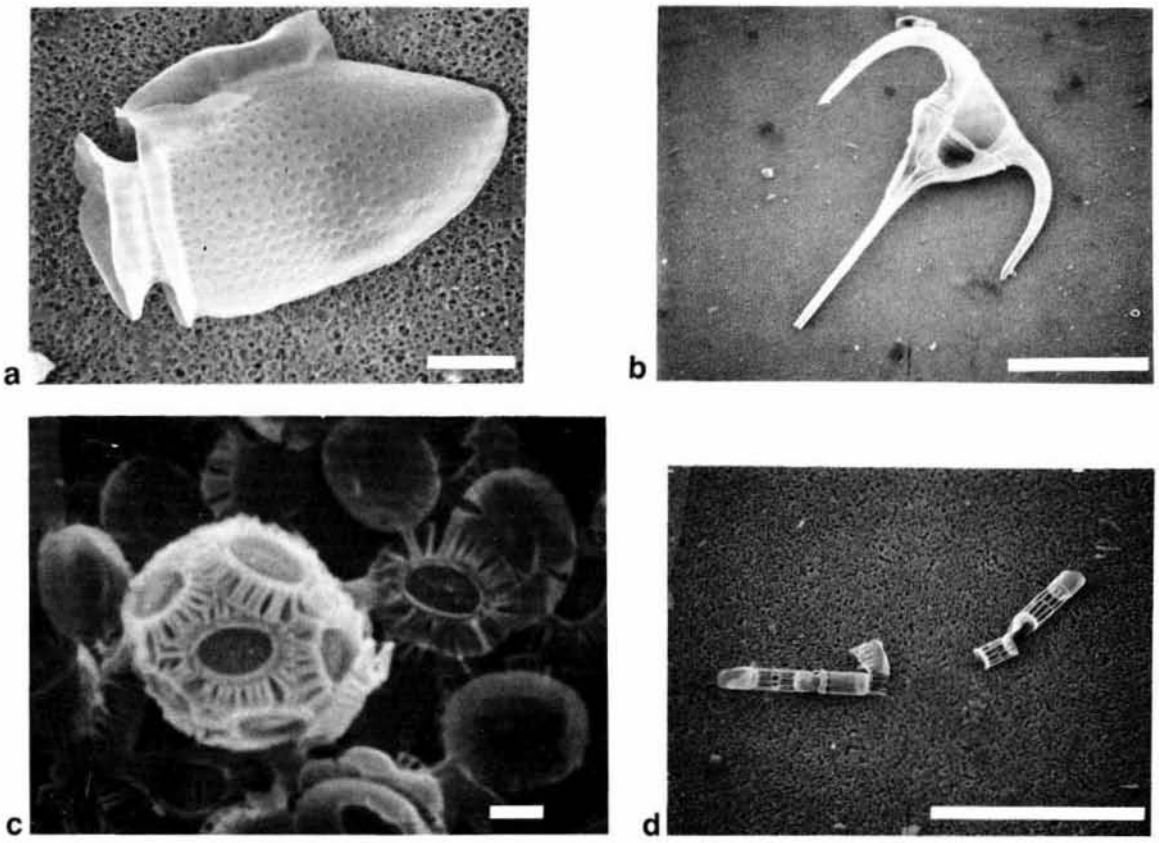

Plate 1

Biogenic components of the particulate matter. a) Dinophysis *sp. (dinoflagellate) ; b)* Ceratium *sp. (dinoflagellate); c)* Emiliania huxleyi *(coccoliths and coccosphere); d)* Skeletonema *sp. (diatom).*

Constituants biogènes de la matière particulaire. a) *Dinophysis* sp. (dinoflagellé); b) *Ceratium* sp. (dinoflagellé) ; c) *Emiliania huxleyi* (coccolithes et coccosphère) ; d) *Skeletonema* sp. (diatomée).

fractions smaller than 8 µm (dominated by clays) and those between 8 and 24 µm (many clay aggregates) increase correlatively. Although the particle sizes decrease, the amount of particles increases only a little, reflecting a decline in particulate concentration. The bulk suspended load does not significantly vary because the decrease of the amount of particles (130 to 144 x 10^4 l^{-1}) is equilibrated by an increase of the density of the particulate material (mineral particles). In the above levels, the particulate density is lower because of the abundance of biogenic components of planktonic origin.

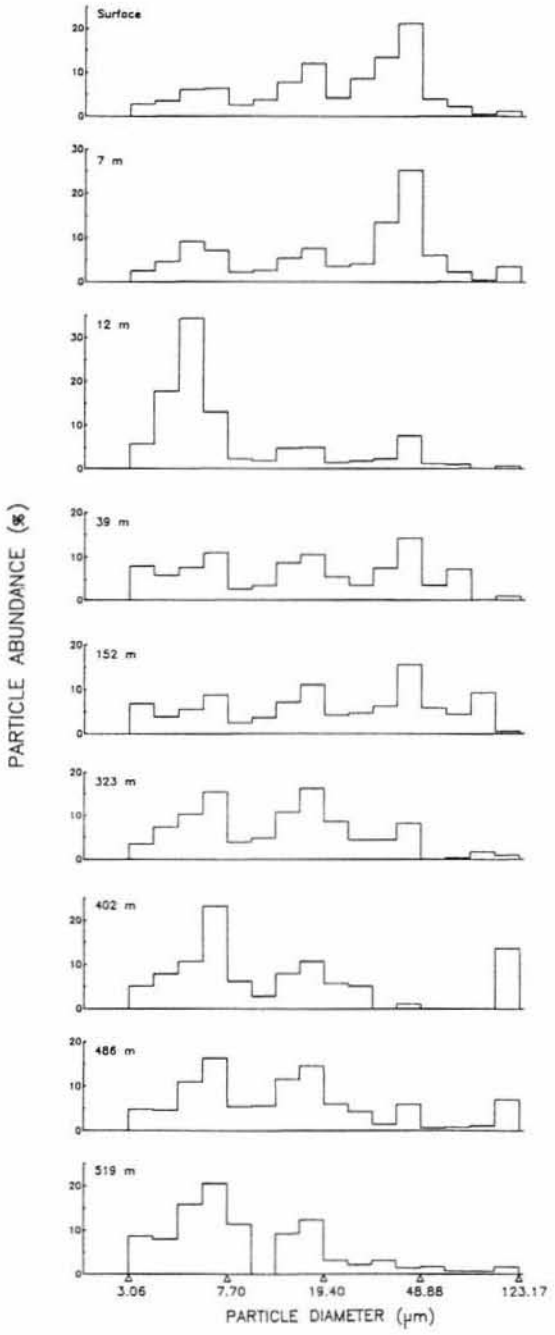

Figure 5

Suspended matter grain-size distribution.

Distribution granulométrique de la matière en suspension.

486 m depth

The peak of turbidity (0.84 NTU) at this level is associated with a slight increase of the particle volumic concentration (0.35 mm^3 l^{-1}) and of the suspended load (0.71 mg l^{-1}). The clay aggregates become more abundant. Mineral particles of authigenic origin are also observed; we shall later return to these materials. In bulk, the mineral fraction becomes predominant.

519 m depth

The particulate material is similar to that described at 486 m depth, with a far more pronounced abundance of the clay aggregates (4-8 µm fraction).

The mineral particles observed at 486 and 519 m depth and, to a lesser extent at 402 and 323 m depth, display a substantial Fe and Mn enrichment. These particles exist in three different forms:

- ring structures, with a diameter similar to that of coccoliths (Pl.2 *b-c*), suggesting that such calcareous tests could act as supports for Fe-Mn coatings;

- rodlike particles, isolated or accumulated as colony (Tab. 2 *b-e*), resembling bacteria in shape and size;

- flowerlike particles, isolated or associated with clay aggregates (Pl. 2. *d-e*), which could result from the crystalline development of the previous structures.

The genesis of these striking particles is discussed further in the light of counting and geochemical results.

Particle geochemistry

The results of the neutron activation analyses are shown in Table 1, together with the results of particulate C and N measurements.

Element composition displays large variations all along the water column (Fig. 6-7). Comparison between Al and Sc contents in the particles and those given in shales indicates that the proportion of the alumino-silicate phase, as it can be identified by these two key elements, is relatively small: it can reach 15-20 % in the sample collected at 519 m depth. Many elements show concentration profiles very similar to those observed for Sc and Al: this is the case for Cs, Th, La, Ce, Eu (Fig. 6). Therefore, these elements seem to be poorly involved in either biogenic or authigenic phases. Consequently, we shall consider as a first approximation that these elements are primarily associated with the clay minerals. This inference is supported by the consistency of their contents along the profiles with those in shales (corrected by a 0.15 factor) as represented by the vertical dotted lines in Figure 6. Additionally, the correlation between Al and Sc contents is straightforward ($r^2 = 0.95$). However, the mean Al/Sc ratio (3 700 ± 400), deduced from the regression line, is much lower that the ratio which would be expected for shale-type material, that is about 6 800. This observation suggests that the local geochemical background could be characterized by a remarkable depletion of Al (48 000 µg g^{-1} instead of 88 000 µg g^{-1} in shales). Price and Skei (1975) also reported Fe/Al ratios of about 1 (Fe/Al ≈ 0,5 in shales),

Plate 2

Detrital and authigenic components of the particulate matter. a) Fe-hydroxide coated clay particle; b) Mn-rich ring structure and rodlike particles; c) Mn-rich ring structure; d) mn-rich flowerlike particles; e) rodlike and flowerlike particles associated with clay aggregates.

Constituants détrétiques et authigènes de la phase particulaire. a) particules argileuses avec enduits d'hydroxyde de fer ; b) structure en anneau et particules en bâtonnets ; c) structure en anneau ; d) particules en rosettes ; e) particules en bâtonnets et en rosette associées à des agrégats argileux.

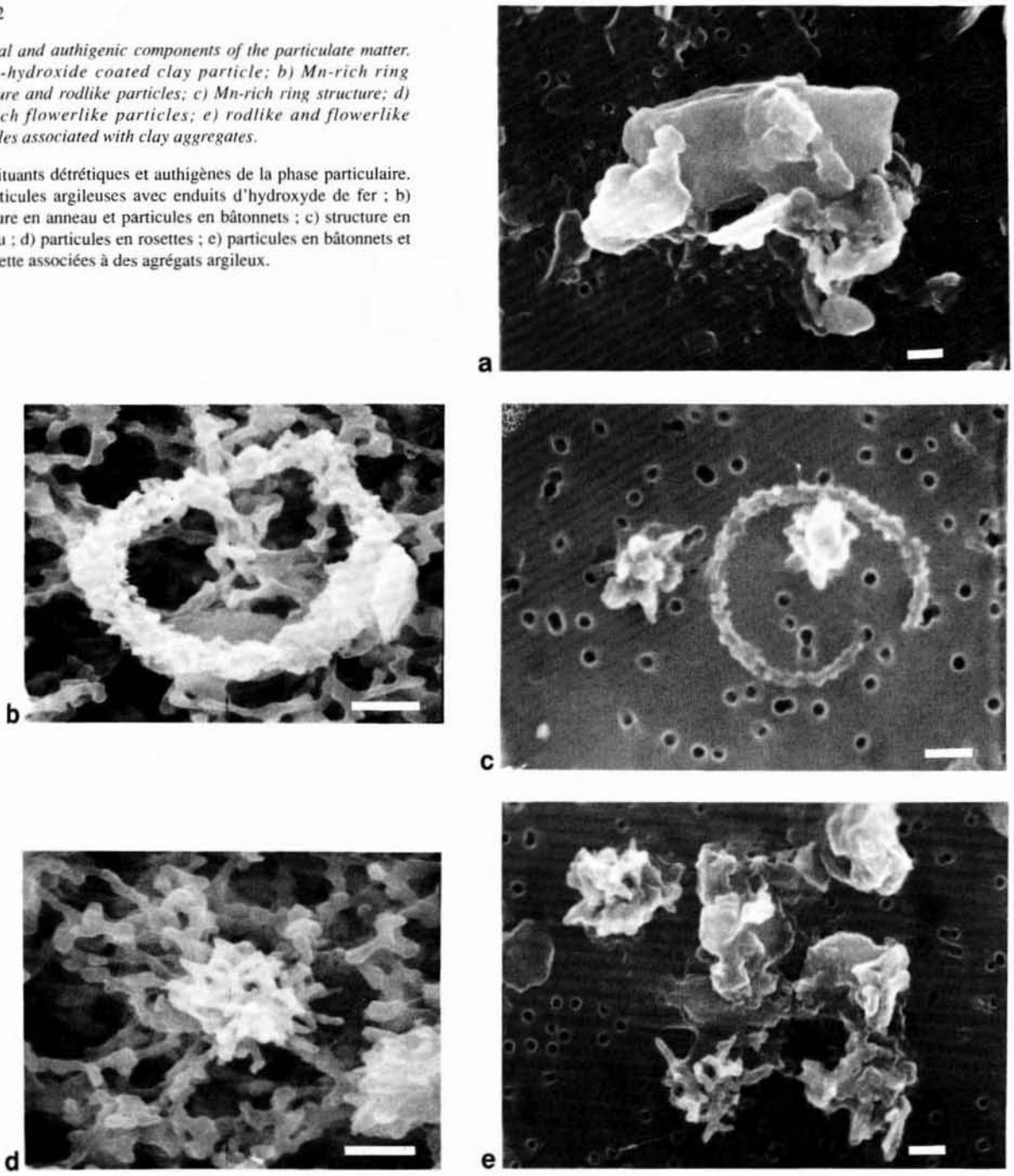

for the detrital particulate matter of the Hardangerfjord (Norway).

The profiles of particulate Mn, Fe, Co and Zn are significantly different from those of Sc and Al (Fig. 7). In addition, all these elements are enriched with respect to the shale reference. Therefore, the influence of other lithologic phases than clays must be assumed to account for these observations. For each of these elements and at each level along the water-column, we have calculated the contribution of the alumino-silicate phase (detrital material assumed to be shale-type material) from the Sc content. This calculation allows us to determine the element content which is in excess relative to shales, and then, to quantify the contribution of the other phases which must be identified.

The content of an element E in the alumino-silicate phase is :

$E_D = E_T\ (Sc_T \times (E/Sc)_{SH})$

where E_T is the content of the element E in the bulk sample, Sc_T the Sc content in the bulk sample, and $(E/Sc)_{SH}$ the shale normalized E/Sc ratio.

The results are reported in Table 2 and Figure 7. They indicate that the variation of the alumino-silicate phase abundance cannot account for the variation of Mn, Fe, Co, and Zn contents. Mn is by far the most enriched element. The contribution of the alumino-silicate phase for this element never exceeds 200 $\mu g\ g^{-1}$. Consequently, the quantity of Mn which is not associated with alumino-silicates is largely predominant (Tab. 2). This point will be discussed below.

Table 1

Elemental composition of the particulate matter at station 106; values are in µg g^{-1} unless otherwise stated; POC and PON are particulate organic carbon and nitrogen, respectively.

Composition élémentaire de la matière particulaire à la station 106 ; les valeurs sont en µg g^{-1} sauf autre indication ; POC et PON représentent respectivement le carbone et l'azote organiques particulaires.

Depth (m)	Al	Sc	Mn	Fe	Co	Zn	Rb	Cs	La	Ce	Eu	Th	P.O.C. (%)	P.O.N. (%)	C/N
1	-	-	-	-	-	-	-	-	-	-	-	-	2.50	0.31	8.1
7	825	0.05	182	-	0.8	67	-	-	-	-	0.02	-	6.03	0.40	15.1
39	3394	0.68	417	2510	5.1	22	-	-	3	6	0.09	0.70	-	-	6.4
152	7722	1.95	1069	8292	7.6	62	-	1.04	11	12	0.22	1.97	3.53	0.41	8.6
323	9109	2.16	5090	20304	12.4	75	-	1.2	11	18	0.28	2.21	2.36	0.64	3.7
402	5504	1.54	4282	16092	9.5	105	-	0.7	3.5	10	0.19	1.42	3.38	0.75	4.5
486	4746	1.43	10358	20243	10.2	136	-	0.7	-	11	0.20	1.29	1.43	0.39	3.7
519	11704	2.89	32326	35333	19.1	161	25	1.5	23	23	0.31	2.44	3.09	0.41	7.5

Table 2

Amount of element unsupported by shale abundance calculated on Sc basis (in µg g^{-1} and % of the total element).

Quantité d'élément inexpliquée par l'abondance d'un matériel de type shale calculée grâce à Sc (en µg g^{-1} et en % de l'élément total).

Depth	Mn_x		Fe_x		Co_x		Zn_x	
(m)	µg g^{-1}	%	µg g^{-1}	%	µg g^{-1}	%	µg g^{-1}	%
7	181	99	-	-	0.8	96	67	100
39	373	89	10	0	4.1	80	17	77
152	942	88	1062	13	4.8	63	48	77
323	4950	97	12295	61	9.2	75	59	79
402	4182	97	10382	65	7.3	58	94	89
486	10265	99	14941	74	8.1	80	116	92
519	32138	99	24617	70	14.9	78	140	87

DISCUSSION

The Baltic outflow : physical and biological processes

The data reported here clearly illustrate the occurrence of a highly stratified water column, characterized by steep salinity-temperature gradients at 20 m depth. This yields the superposition of two water masses of different origin, namely the Baltic Sea and the North Sea. The low turbidity encountered in the water column (< 1 NTU) and, consequently, the light penetration, would favour phytoplankton to grow throughout the topmost 50 m waters. Living forms of phytoplankton are however only observed within the Baltic waters (topmost 20 m) in which we observed two superposed layers corresponding to optimal conditions of two major phytoplankton groups: Dinoflagellates (1 m and 7 m depth samples) and Coccolithophoridae (12 m depth sample).

Dinoflagellates are mainly represented by Ceratidae, Goniolacidae, Peridinidae and Dinophysidae. Larger sized Ceratidae account for the major part of the > 25 µm fraction, with a maximum in the range 30-50 µm. Smaller sized species, such as *Dinophysis* sp., fall in the 10-25 µm fraction.

The theca (or amphiesma) of the dinoflagellates is composed of cellulosic plates (Sournia, 1986). Cellulose is quasi-insoluble in seawater in so far as specific cellulolytic microflora is not active. As a result, the dinoflagellate thecae are preversed without any further alteration throughout the water column (Anderson *et al.*, 1985). During the *Tramanor* cruise, they were observed throughout the North Sea, at all depths, with a pronounced maximum in surface waters (living organisms).

The optimal growing zone for Coccolithophoridae occurs a little deeper (12 m depth) and is characterized by the increase of the abundance of the < 10 µm fraction, mainly consisting of *Emiliana huxleyi* coccospheres (6-7 µm in diameter). The phytoplankton bloom is located above the frontal structure as reported by Holligan *et al.* (1983) and Houghton (1988) and is characterized by the particle concentration (number l^{-1}) profile (Fig.4). Morever, as phytoplankton maxima have been observed at similar depths but not necessarily coupled with frontal structures, the Coccolithophoridae accumulation above the halocline is due to both occurence of optimal growing conditions and settling of coccospheres through a strong salinity gradient. One cannot find living Coccolithophoridae below the halo-

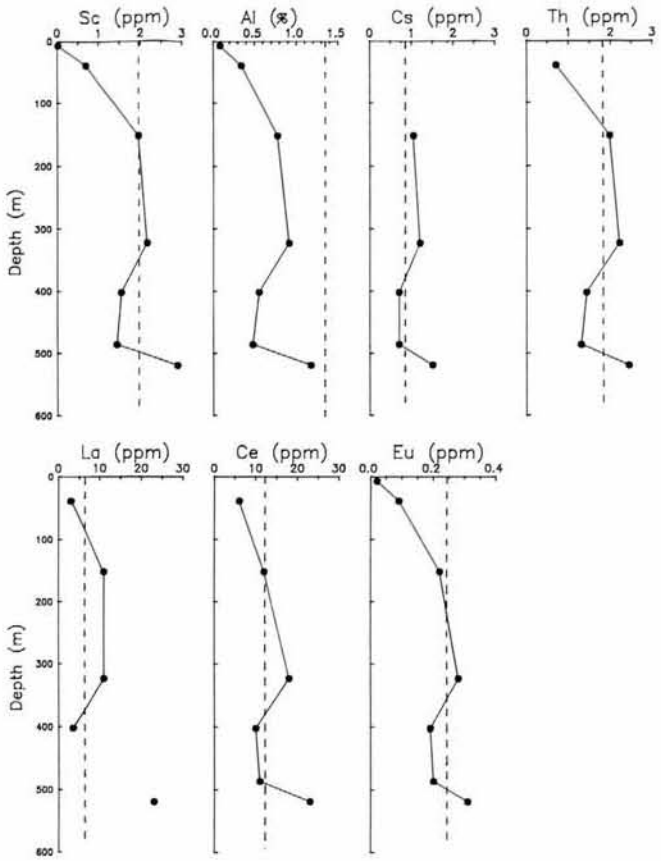

Figure 6

Detrital phase element composition. The vertical dotted line represents 0.15 average shale concentrations (from Wedepohl, 1968).

Composition élémentaire de la phase détritique. La ligne verticale en pointillés représente 0,15 fois les concentrations moyennes dans les shales (d'après Wedepohl, 1968).

cline; furthermore, coccoliths are likely to undergo active desaggregation and/or dissolution in deeper samples.

Dinoflagellates and particulate geochemistry

Due to their predominance in the > 30 µm fraction, the abundance of dinoflagellates in each sample can be estimated, as a first approximation, by the abundance of the > 30 µm fraction, and thus, compared to other sensitive geochemical parameters (Tab. 3). As dinoflagellate thecae are composed of cellulose (a compound devoid of nitrogen), the increase of POC at 7 m depth, up to 6.03 % is not surprising, while PON remains fairly constant (Fig. 8) and C/N ratio reaches 15.1. Due to the conservative behaviour of cellulose in the water column, the relative abundance of dinoflagellates must have a major influence on C/N ratios. A simple mixing model between cellulose (without PON) and old marine organic matter having the lowest C/N ratio observed in the profile (C/N = 3) should account for the data. In Figure 9, N/C ratios (instead of C/N ratios to get linear regression) have been plotted *versus* Dinoflagellate abundance. Almost all the data points fall under those predicted by the mixing model. The best fit line ($r^2 = 0.95$, when 519 m point is discarded) intercepts the x-axis at 65 %, suggesting that the dinoflagellate abundance is underestimated, particularly for high C/N values. This is not surprising because a certain amount of dinoflagellates is found in smaller grain-size fractions (10-25 µm; *Dinophysis* sp.) and, therefore, can be estimated this way (Tab. 3). This explanation does not hold for the 519 m depth sample: the C/N ratio clearly reflects resuspension of surficial sediments (C/N ≈ 15 - 20; Blackburn and Henriksen, 1983) as confirmed by SEM observations of clay organic-rich aggregates.

The profile of Zn excess (*see* Tab. 2) suggests that particulate Zn concentrations are influenced by both Mn-rich particles (downwards increase stated in the Results section)

Table 3

Estimation of the amounts of dinoflagellates in different size fractions: 1) assumed to consist mainly of dinoflagellates; 2) estimated from mixing model (see Fig. 9) unless stated; 3) no dinoflagellate is observed in the < 30 µm fraction using SEM; 4) mainly consisting of Dynophysis *sp. in the 10-25 µm fraction.*

Estimation des quantités de dinoflagellés dans différentes classes de taille : 1) principalement constituée de dinoflagellés ; 2) estimée d'après le modèle de mélange (*cf.* fig. 9), sauf autre indication ; 3) pas de dinoflagellés dans la fraction < 30 µm ; 4) essentiellement constituée de *Dynophysis* sp. dans la fraction 10-25 µm.

Depth (m)	Abundance of the > 30 µm fraction % (1)	Dinoflagellates % (2)	Dinoflagellates in the < 30 µm fraction % (4)
1	42	55	13
7	51	75	20
39	33	45	12
152	42	57	15
323	15	15 (3)	0
402	15	27	12
486	17	17 (3)	0
519	3	3 (3)	0

Figure 7

Vertical profiles of particulate enriched-element concentrations. Dotted lines as in Figure 6; ●*: measured values;* ❍*: shale-supported contribution (see text); 188 ppm maximum for Mn.*

Profils verticaux des concentrations particulaires en éléments enrichis. Lignes en pointillés comme sur la figure 6 ; ● : valeurs mesurées; ❍ : contribution des shales (*voir* texte); 188 ppm maximum pour Mn.

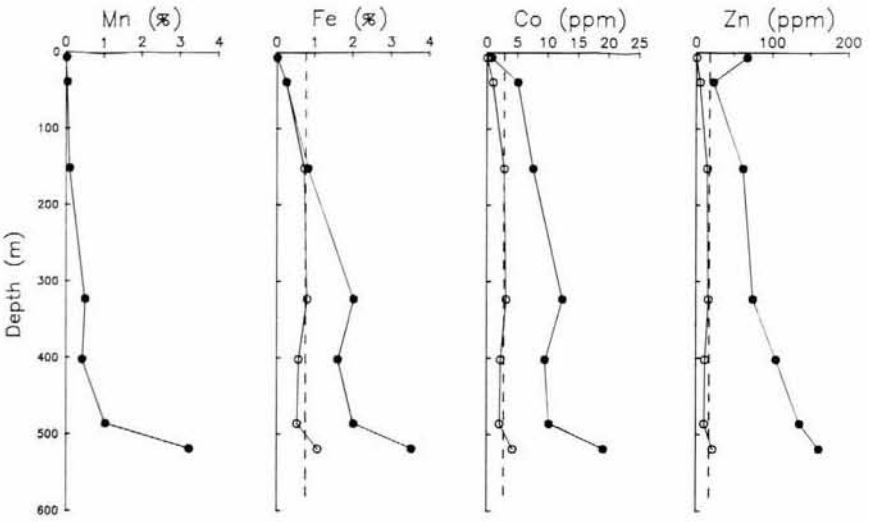

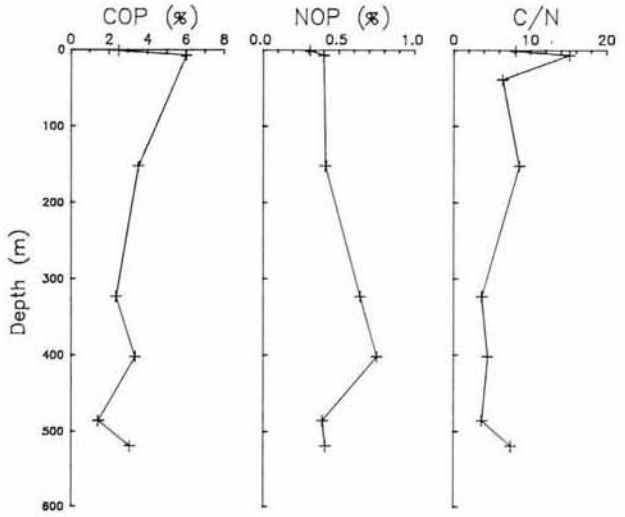

Figure 8

Particulate organic carbon, nitrogen and C/N profiles.

Profils de carbone et d'azote organiques particulaires, et du rapport C/N.

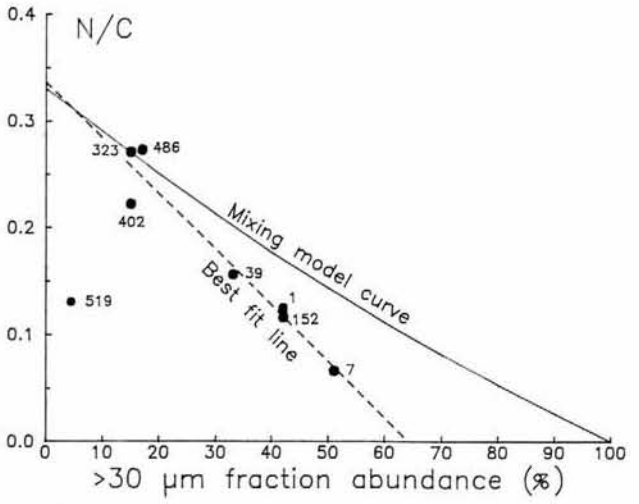

Figure 9

N/C ratio versus *> 30 µm fraction abundance. Point labels refer to sampling depth.* See *text for explanation of the mixing model. 519 m sample discarded for data best-fit line.*

Rapport N/C en fonction de l'abondance de la fraction > 30 µm. La numérotation des points représente la profondeur d'échantillonnage. *Voir* texte pour l'explication du modèle de mélange. L'échantillon à 519 m a été écarté pour le calcul de la droite de régression.

and dinoflagellate abundance (Fig. 10); this is especially observed for the 7, 39 and 152 m depth samples and, perhaps, for the 402 m depth sample. Moreover using the linear relationships between Zn_x and total dinoflagellate abundance (Tab. 3), illustrated on Figure 11, one can estimate the Zn concentration of the dinoflagellate cells is about 100 µg g^{-1}. The x-axis intercept of the linear regression shows that a certain part of the inferred dinoflagellate population does not hold any Zn excess. This could reflect the proportion of non-living cells but no definite conclusion can be drawn as far as Zn adsorption mechanism into the cellulose structures is not elucidated: biological uptake as known for chitin (another polysaccharide) or physical adsorption.

Detrital components

Al and Sc are often considered as good markers of the alumino-silicate fraction of marine sediments, and, therefore, of clay abundance. In many cases, clays are the dominant lithological fractions in the detrital components contained in the sediments. Moreover, Al and Sc are poorly mobilized throughout ocean processes as they are strongly associated with the clay lattice. As a result, they are both assumed to be conservative markers of the detrital phase of the sediments. In our samples, Al and Sc are strongly correlated ($r^2 = 0.97$) and should be mainly contained within clay minerals as they are from far the most abundant aluminosilicate phase. Our sampling strategy allows us to assess this often-unchecked assumption. We directly measured the area occupied by clay minerals on SEM photographs; this seemed to be a better basis than particle counting because of the wide range of clay grain-size (*ca* 0.5-20 µm). Clay abundance, estimated in μm^2, correlates fairly well with Sc particulate concentrations (Fig. 12). Only the 486 m sample falls far off the previous relation due to a great (and unexplained) overestimation of the clay abun-

Figure 10

Vertical profiles of Zn excess concentrations (■) and dinoflagellate abundance (●).

Profils verticaux des concentrations en Zn en excès (■) et de l'abondance des dinoflagellés (●).

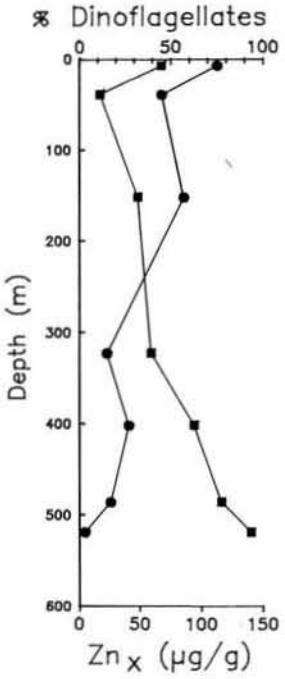

Figure 11

Excess Zn concentration versus *dinoflagellate abundance for the three uppermost samples (% dinoflagellates > 45).*

Concentration de Zn en excès en fonction de l'abondance en dinoflagellés pour les trois premiers échantillons (% dinoflagellés > 45).

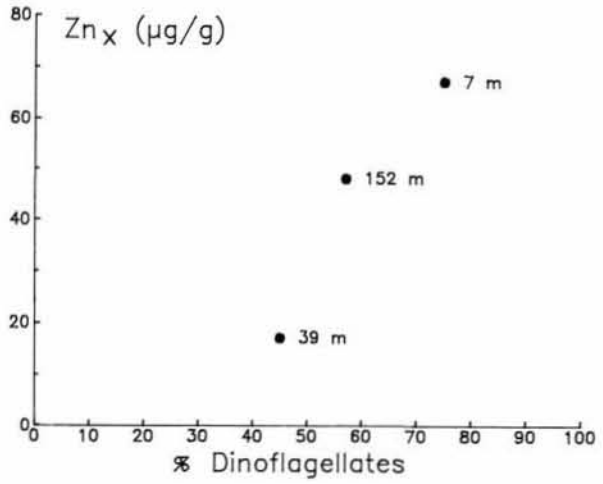

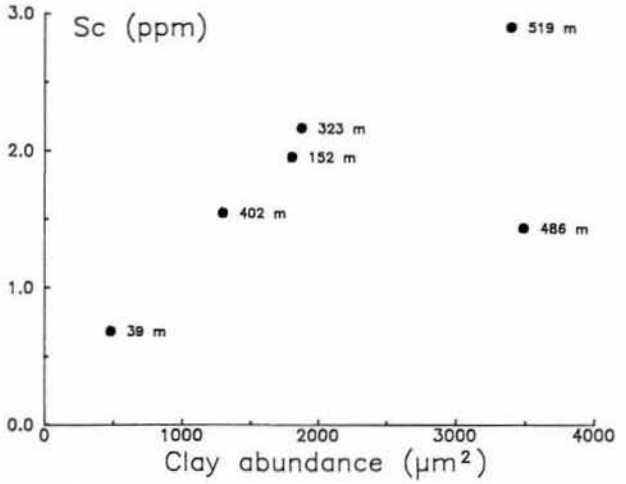

Figure 12

Particulate Sc concentrations versus clay abundance estimated from the surface area (µm²) of clay minerals measured on SEM photographs.

Concentrations en Sc particulaire en fonction de l'abondance des argiles estimée à partir de la surface des minéraux argileux mesurées sur les photographies au MEB.

dance. Despite this discreapancy, the SEM and NAA data display a very nice consistency. Furthermore the Sc-clay area relationship holds only because the area to mass ratio of all collected clay particles is constant.

When plotted *versus* Sc, conservative elements (Al, Cs, Ce, Eu and Th) display correlation coefficients greater than 0.90 (Tab. 4, only 0.74 for La). As intercepts of the regression lines are not significantly different from zero, their slope are representative of the average Sc-normalized concentrations of each element, which are therefore compared to average shale (Tab. 4). The agreement between the two sets of data is fairly good (except for Al, *see* above). Briefly, the detrital component of the suspended load is mainly made of a chemically homogenous pool of shale-type minerals.

Authigenic processes

The occurrence of highly Mn-enriched particles at almost any levels throughout the water column and the huge

Table 4

Chemical characterization of the detrital component of the suspended load of station 106: 1) correlation coefficient of the element versus *Sc; 2) slope of the regression line of element* versus *Sc; 3) Wedepohl (1968).*

Caractérisation chimique de la composante détritique de la matière en suspension de la station 106 : 1) coefficient de corrélation de l'élément par rapport à Sc ; 2) pente de la droite de régression entre l'élément et Sc ; 3) Wedepohl (1968).

	r^2 (1)	a (2)	Sc-normalised shale composition (3)
Al	0.97	3800 ± 400	6800
Cs	0.97	0.6 ± 0.1	0.42
Ce	0.92	8 ± 1	6.2
Eu	0.97	0.11 ± 0.03	0.12
Th	0.95	0.8 ± 0.2	0.92

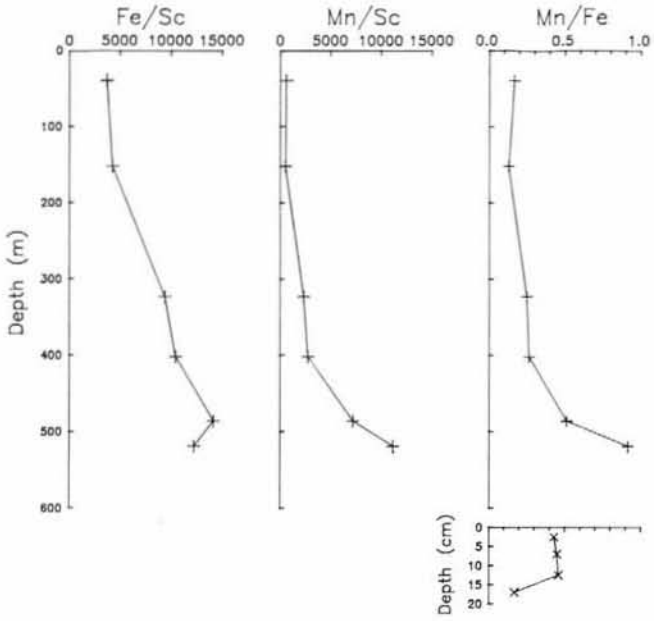

Figure 13

Fe/Sc, Mn/Sc and Mn/Fe ratios in the particulate matter versus *depth. A Mn/Fe ratio profile is also given in the upper sediment column (note different depth scale) at neighbouring station 11 of Rajendran (1986; see Fig. 1).*

Rapports Fe/Sc, Mn/Sc et Mn/Fe dans la matière particulaire en fonction de la profondeur. On donne aussi le rapport Mn/Fe dans la colonne sédimentaire (remarquer l'échelle de profondeur différente) à la station voisine 11 de Rajendran (1986; *voir* fig. 1).

Figure 14

Particulate Mn (○) and Mn-rich particle abundance (□) profiles as determined from SEM photographs.

Profils de Mn particulaire (○) et d'abondance des particules riches en Mn (□) déterminée sur des photographies au MEB.

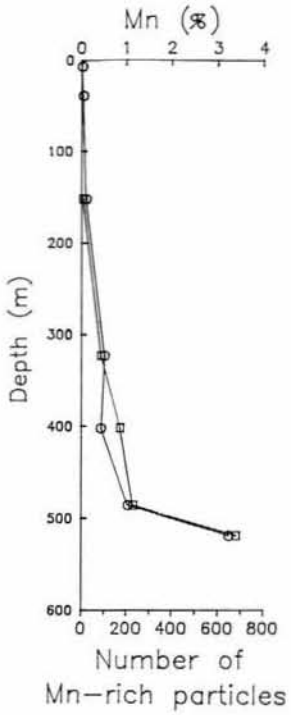

increase of particulate Mn at depth and, to a lesser extent of particulate Fe, is a very attractive feature among the observations reported here (Fig. 7). This kind of particles has been described in a wide variety of environments, and especially in fjords (Robb, 1981 ; Skei and Melsom, 1982 ; van der Sloot *et al.*, 1988). The Mn particles originate from enrichment processes which can take place at the sampling station as well as at remote locations, including fjords. Export of Mn-rich particles either from shallow-water energic environments or from neighbouring fjords, such as Bunnefjord, off Oslo, investigated by Skei and Melsom (1982), is yet to be supported by the observations at present. The head of this fjord is at only some 200 km to the NNE of our sampling station. This mechanism, if it occurs, is probably of least importance because unherited particles should have higher Mn/Fe ratios than those measured at station 106 (Fig. 13). In addition, despite of a certain analogy, the Mn particles of this fjord do not display the same morphological types. As previously pointed out by Eisma (1981) and Skei (1981), the supply of particulate matter remains largely inside the fjords. Whatever their provenance, the Mn-rich particles can be accounted for precipitation processes taking place (1) within the column and/or (2) in the bottom water.

In the former case, dissolved Mn^{2+} diffuses upwards under reducing conditions, precipitates in the top oxic layer of the sediment, Mn enriched particles are then resuspended by bottom currents. Data reported in Figure 13 allow us to test this hypothesis by the comparison of Mn/Fe ratios in particulates and in surface sediments collected by Rajendran (1985; station 11, Fig. 1). In the core 11 of this author, the oxygen penetration depth is 15 mm. This induces a Mn-precipitation front which is easily detectable (sampling interval of ca 5 mm) yielding Mn/Fe ratios of ≈ 0.45. While this kind of process can probably account for the slight Mn and Fe enrichment at 323 and 402 m depth, as denoted by Mn/Sc and Fe/Sc profiles (Fig. 13), it is not able to explain the great increase of particulate Mn in the two deepest samples (486 and 519 m depth). The Sc-normalized concentrations of Fe only increase by a factor of 1.2 between 402 and 519 m depth while those of Mn increase four-fold in the same depth interval. This strongly suggests a Mn-specific process.

In the latter case, Mn^{2+} can diffuse from the interstitial water to the bottom water and then be reprecipitated as Mn-oxides onto the suspended matter (Sundby, 1977; Sundby *et*

Table 5

Results of Mn-rich particle countings, expressed as number of particles per 0.01 mm², and as % of different types between parentheses; the filter surface counted ranges between 0.01 and 0.02 mm².

Résultats des comptages de particules riches en Mn, exprimés en nombre de particules par 0,01 mm², et en % des différents types entre parenthèses ; la surface de filtre comptée varie de 0,01 à 0,02 mm².

Depth (m)	Flowerlike particles	Rodlike particles	Ring structures	Total
7	-	-	-	-
39	-	-	-	-
152	7 (88)	-	1 (12)	8
323	9 (10)	53 (61)	25 (29)	87
402	18 (10)	107 (62)	48 (28)	173
486	9 (4)	174 (76)	47 (20)	230
519	23 (4)	621 (91)	36 (5)	680

al., 1981; Price and Skei, 1975; Skei and Melsom, 1982). These processes take place under and above the redox boundary layer, respectively, and are driven by both redox conditions (*i.e.*, oxygen penetration in the sediment-column) and the kinetics of the reprecipitation of Mn^{2+} on to particles as Mn^{3+}. In the light of the above argument, the two processes invoked are likely to occur simultaneously; their relative importance clearly depends on the oxygen penetration depth and on hydrodynamic conditions.

The contrasting behaviour of Mn *versus* Fe is clearly supported by the relative reactivity of these two elements: 1) the reduction of solid Fe^{3+} to soluble Fe^{2+} in anoxic sediments occurs deeper in the sediment column when compared to Mn; 2) the kinetics of Fe oxidation and its readsorption on to particles is much faster than for Mn (Horowitz *et al.*, 1973; Troup *et al.*, 1974; Hirst and Aston, 1983).

The counting of each type of Mn-rich particles gives rise to a better insight on the sampling reliability and on the genesis of these particles. The abundance of each particle type, expressed as number of particles per unit surface (0.01 mm^2) are given in Table 5 and plotted *versus* depth on Figure 14, together with bulk particulate Mn concentrations. There is a big increase of the number of Mn-rich particles almost parallel to that of total Mn.

In addition, rodlike particles are dominant (60 to 91 %) at any level deeper than 152 m. No Mn-rich particle of any type are detected in surface samples, nor at 7 and 39 m levels. Therefore, it can be concluded that the particulate Mn concentration is mainly dependent on the abundance of rodlike particles and, to a lesser extent, of ring structures. The great increase of the number of rodlike particles from 486 m (174) through 519 m (621) suggests that these excess particles mainly originate from the local authigenic processes described above, while ring particles could be advected from adjacent areas. This could be further investigated by morphometric inspection of these particles.

The Mn-rich ring structures have been already described in fjord systems (*e.g.* van der Sloot *et al.*, 1988), lakes (Mudroch and Bistricki, 1981), or nodules (Janin, 1987). They were sometimes interpreted as the result of Mn-precipitation on to coccoliths. Morphometric analyses of both ring structures and coccoliths (*Emiliana huxleyi*) reveals significantly different mean diameters of 3-5 and 6-7 µm, respectively. From this observation, it is clear that coccoliths observed in the upper water column (Baltic outflow) are not involved in the inferred authigenic processes which yields ring structures observed lower in the column. Nevertheless, the precipitation of Mn on to coccoliths could be initiated by morphotypes of *Emiliana huxleyi* of larger size (Pujos-Lamy, 1976) as those observed in the Dover Strait and off Dutch coast, or by coccoliths of the *Gephyrocapsa* sp. group. This again suggests that Mn-rich particles are likely to be advected to the site with water masses flowing from the Southern North Sea. As a consequence, only bottom samples are likely to be influenced by strictly local authigenic processes.

CONCLUSION

From our findings, it becomes clear that it is very promising to collect marine particle samples in order to obtain relevant physical and chemical parameters, provided that the reliability of the data and the sample-subsample homogeneity are ensured as far as possible. The cross-comparison of independently obtained parameters on different subsamples and the accuracy of the interpretation fully enhance the consistency of both analytical work and particle sampling strategy.

In summer conditions (July 1988), the particulate matter of the Baltic outflow (20 m topmost water column) was found to undergo a plankton bloom, dominated by dinoflagellates and Coccolithophoridae. Below the halocline, almost no living cells were found. By combining Coulter analyses, SEM observations and particulate organic C and N data, the abundance of dinoflagellates was estimated and their influence on Zn biological recycling clearly stated.

The detrital components mainly consist of clay minerals. Moreover, the abundance of clay, determined by particle-counting, closely correlates with Sc (and Al, Cs, La, Ce, Eu, Th) concentrations. The detrital phase is assumed to have a rather constant mineralogy throughout the water column.

On the other hand, Mn, and Fe, Co and to a lesser extent Zn, are highly enriched in particles. Excess element (non-supported by shale-type material abundance) increases dramatically at depth, especially Mn. The concentrations of these elements correlate with the abundance of Mn-rich particles determined by counting. At least some of these Mn-rich particles are likely to form locally by diffusion of dissolved Mn from interstitial waters, and subsequent precipitation on to particles. This process could be effective for other trace-metals which would therefore be efficiently scavenged and removed from seawater.

Acknowledgements

The authors are grateful to the scientific party of the *Tramanor* cruise and to the crew of the R.V. Cryos. We are indebted to Mr Bigois (*Service Central d'Analyses, CNRS*, Vernaison) who provided POC and PON measurements. Neutron activation analyses were performed at the *Laboratoire Pierre Süe* in Saclay. Some of the gamma-countings were provided by Y. Baron (*Groupe d'Études Atomiques, Marine Nationale*). We thank Drs C. Lambert, P. Buat-Ménard, R. Delmas, F. Dulac and A. Véron for their efficient technical and scientific participation in this study. Mrs I. Zimmerlin (*Université de Rouen*) and Mr J. Breton (Bureau de Recherches Géologiques et Minières, Orléans) are thanked for their helpful assistance in SEM operations. The manuscript has benefited from constructive comments by Dr W. Helder. The typing expertise of Mrs. Leconte was appreciated.

REFERENCES

Anderson D.A., J.J. Lively, E.M. Reardon and C.A. Price (1985). Sinking characteristics of Dinoflagellate cysts. *Limnol. Oceanogr.*, **30**, 1000-1009.

Aure J. and R. Saetre (1981). Wind effects on the Skagerrak outflow. in : *The Norwejian Coastal Current*, R. Saetre and M. Mork, editors, University of Bergen, 263-294.

Blackburn T.H. and K. Henriksen (1983). Nitrogen cycling in different types of sediments from Danish waters. *Limnol. Oceanogr.*, **28**, 477-493.

Dahl F.E. (1978). On the existence of a deep contercurrent to the Norwegian coast current in Skaggerak, *Tellus*, **30**, 552-556.

Dooley H.D. (1974). Hypotheses concerning the circulation of the northern North Sea, *J. Cons. int. Explor. Mer*, **36**, 54-61.

Eisma D. (1981). Supply and deposition of suspended matter in the North Sea. *Spec. Publ. Int. Ass. Sed.*, **5**, 415-428.

Eisma D. and J. Kalf (1987). Dispersal, concentration and deposition of suspended matter in the North Sea. *J. geol. Soc., Lond.*, **144**, 161-178.

Furnes G.K., B. Hackett and R. Saetre (1986). Retroflection of Atlantic water in the Norwegian trench. *Deep-Sea Res.*, **33**, 247-265.

Hirst J.M. and C.R. Aston (1983). Behaviour of copper, zinc, iron and manganese during exprimental resuspension and reoxidation of polluted anoxic sediments. *Estuar. coast. Shelf. Sci.*, **16**, 540-558.

Holligan P.M., M. Viollier, D.S. Harbour, P. Camus and M. Champagne-Philippe (1983). Satellite and ship studies of coccolithophore production along continental shell edge. *Nature*, **304**, 339-342.

Horowitz R.M., L.S. Waterman and W.S. Broecker (1973). Interstitial water studies, leg 15, new procedures and equipment: *Initial Repts. Deep Sea Drilling Proj.*, **20**, 757-763.

Houghton S.D. (1988). Thermocline control on coccolith diversity and abundance in recent sediments from the Celtic Sea and English Channel. *Mar. Geol.*, **83**, 313-319.

Janin M.-C. (1987). Micropaléontologie de concrétions polymétalliques du Pacifique central : zone Clarion-Clipperton, chaîne centre Pacifique, île de la Ligne et archipel des Tuamotu (Eocène-Actuel). *Mém. Soc. géol. Fr.*, **152**, 317 pp.

Ljøen R. (1981). On the exchange of deep waters in the Skaggerak basin. in: *The Norwegian Coastal Current*, R. Saetre and M. Mork, editors, University of Bergen, 340-356.

Ljøen R. and A. Svansson (1972). Long-term variations of sub-surface temperatures in the Skagerrak. *Deep-Sea Res.*, **19**, 227-288.

Moller D. and A. Svansson (1978). Investigations in the Northern Kattegat during the international Jonsdap-76 period Inout, March-April 1976. *Meddelande fran Havsfiske laboratorier. Lysekil n° 243.* Hydrografiska avdelingen, Göteborg.

Mudroch A. and T. Bistricki (1981). Occurrence of manganese-rich microparticles in the eastern bassin of lake Erie. *Can. Mineral.*, **1**, 345-440.

Price N.S. and J.M. Skei (1975). Areal and seasonal variations in the chemistry of suspended particulate matter in a deep water fjord. *Estuar. coast. mar. Sci.*, **3**, 349-369.

Pujos-Lamy A.(1976). *Emiliana* et *Gephyrocapsa* (nannoplancton calcaire) : biométrie et intérêt biostratigraphique dans le Pléistocène supérieur des Açores. *Revta esp. Micropaleont.*, **9**, 1, 69-84.

Rajendran A. (1985). Trace metal geochemistry in three sediment cores from Skagerrak (North Sea), unpublished Report NIOZ, 16 pp.

Robb M.S. (1981). Composition and manganese association of suspended particulate matter at the head of a southeast Alaska fjord, unpublished M.S. Thesis, University of Alaska, Fairbanks.

Salomons W., B.L. Bayne, E.K. Duursma and U. Forstner (1988). *Pollution of the North Sea. An assessment*, Springer Verlag, 687 pp.

Skei J.M. (1981). The entrapment of pollutants in Norwegian fjord sediments. A beneficial situation for the North Sea. *Spec. Publ. Int. Ass. Sed.*, **5**, 461-465.

Skei J.M. and S. Melsom (1982). Seasonal and vertical variations in the chemical composition of suspended particulate matter in an oxygen-deficient fjord, *Estuar. coast. Shelf Sci.*, **14**, 61-78.

Sournia A., J.-M. Brylinski, S. Dallot, P. Le Corre, M. Leveau, L. Prieur and C. Froget (1990). Fronts hydrologiques au large des côtes françaises : les sites-ateliers du programme Frontal. *Oceanologica Acta*, **13**, 4, 413-438.

Sundby B. (1977). Manganese-rich particulate matter in a coastal marine environment. *Spec. Publ. In. Ass. Sed.*, **5**, 461-465.

Sundby B., N. Silverberg and R. Chesselet (1981). Path ways of manganese in an open estuarine system. *Geochim. cosmochim. Acta*, **45**, 3, 293-307.

Troup B.N., O.P. Bricker and J.T. Bray (1974). Oxidation effect on the analysis of iron in the interstitial water of recent anoxic sediments. *Nature*, **249**, 237-239.

van der Sloot H.A., D. Hoede, G. Hamburg, G.J. de Lange, J.J. Middleburg and S. Sophiah (1988). Suspended manganese-rich particles in Kan Bay, Halmahera (Eastern Indonesia). *Mar. Geol.*, **82**, 251-259.

Wedepohl K.H. (1968). Chemical fractionation in the sedimentary environment. in: *Origin and distribution of the elements*, L.H. Ahrens, editor. Pergamon, Oxford, 999-1016.